(e.g. Matsuda et al., 2004). By combining these technical advances with the growing sample of ELANe, one can construct an ideal laboratory to address the scientific questions listed above.

Recognizing this emerging scientific opportunity, we have built an international collaboration to study diffuse gas in emission at $z \sim 2-3$. The team – which includes collaborators F. Arrigoni-Battaia (ESO), S. Cantalupo (ETH), Z. Cai (UCO), B. Emonts (NRAO), D. Fielding (UCB), J. Hennawi (UCSB), C. Martin (Caltech), and K. Stewart (CBU) – combines observational expertise at multiple wave-bands with theoretical expertise in hydrodynamical and radiative transfer (RT) simulations. We have ongoing programs at the Keck, Gemini, VLT, JVLA, ALMA and LBT observatories and will greatly benefit from the recently commissioned KCWI-IFU (Morrissey et al., 2012) on the W.M. Keck II telescope. This grant would fund a full-time PhD student on the project at UC Santa Cruz and partially support the research of a postdoc. It will also engage undergraduates from under-represented populations in forefront research within the LAMAT program at UCSC. Together, we will study diffuse gas in emission to test and refine current paradigms on galaxy formation, AGN emission, and protocluster assembly.

2 Rise of the ELAN

2.1 The Serendipitous Slug

The discovery of our first ELAN – the Slug nebula (Figure 1) – was serendipitous. We observed the field surrounding the ultra-luminous, radio-quiet quasar UM287 with a custom narrow-band filter at its Lyα emission wavelength to search for 'dark' galaxies: extremely faint Lyα emitters (LAEs) fluorescently illuminated by a quasar's ionizing radiation field (Cantalupo et al., 2012). Remarkably, the Slug was well-detected in the first 600 s exposure of our 10-hour integration.

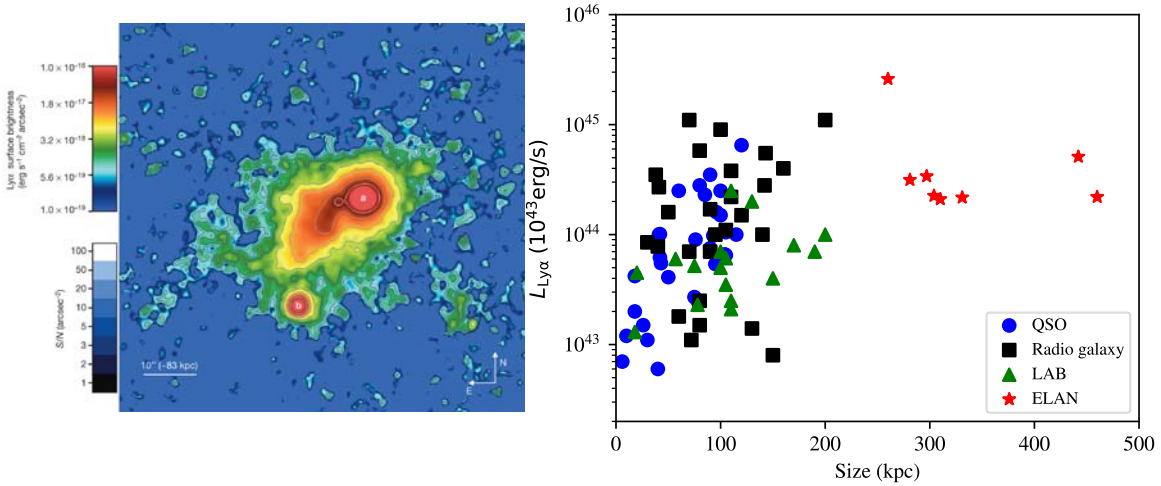

Figure 1: (Left) Lyα image of the Slug ELAN, discovered serendipitously in NB imaging of the ultra-luminous UM287 quasar (marked a). At a surface brightness contour of $10^{-18}\,\mathrm{erg\,s^{-1}\,cm^{-2}\,arcsec^{-2}}$, the ELAN spans over 450 kpc. (Right) Comparison of the sizes and Lyα luminosities of the ELANe described in this proposal with other $z > 2$ Lyα nebulae. This includes nebulae surrounding radio galaxies (black squares), quasars (blue circles), and LABs (green triangles). The ELANe are the extrema of the population. [Adapted from Cantalupo et al. 2014]

The observed Lyα emission of the Slug defines an ELAN: (1) an integrated Lyα luminosity which exceeds 10^{44} erg/s; (2) a spatial extent that exceeds 250 physical kpc; and (3) a peak surface brightness, ignoring point sources, greater than $10^{-17}\,\mathrm{erg\,s^{-1}\,cm^{-2}\,arcsec^{-2}}$. Extended Ly$\alpha$ emission has previously been detected around other $z \sim 2$ sources: radio galaxies, other quasars, and obscured AGN (e.g. Heckman et al., 1991; Venemans et al., 2007) This includes the Lyα blobs (LABs), Lyα nebulae defined to have sizes exceeding 16 arcsec^2 (Matsuda et al.,

2004). Figure 1 (right) compares the Lyα emission of the Slug ELAN (and others discovered by our team) with a set of Lyα nebulae from the literature. The ELANe represent the extreme manifestations of the phenomena. While we suspect that there is commonality between the underlying astrophysics, the ELANe offer a unique opportunity to study cool gas throughout and even beyond the underlying dark matter halo, i.e. into the surrounding intergalactic medium (IGM).

The Slug ELAN is prototypical of the sample and highlights the potential scientific impact. First and foremost, the nebula spans the entire halo of the quasar host galaxy (estimated at $r_{\rm vir} \approx 150\,$kpc) to illuminate the underlying cool gas distribution. This nebula likely includes gas beyond the virial radius, e.g. into the 'filaments' that connect the halo to the cosmic web. Second, the Slug ELAN is sufficiently bright to spatially resolve the gas kinematics, and even non-detections of other nebular lines place constraints on the gas properties and ionization mechanisms (Arrigoni Battaia et al., 2015). Third, the extent and surface brightness of the nebula require a large cool ($T \sim 10^4\,$K) gas mass, M$\sim 10^{11} M_\odot$. Lastly, embedded within the nebula is a luminous AGN which may power the nebula. At the least, the interaction between the ionizing radiation of the quasar and the surrounding gas is fundamental to the observed emission. Furthermore, there is an additional AGN with radio emission towards the SE extension of the nebula; multiple AGNs are a common signature of the ELAN population at least at $z \sim 2$.

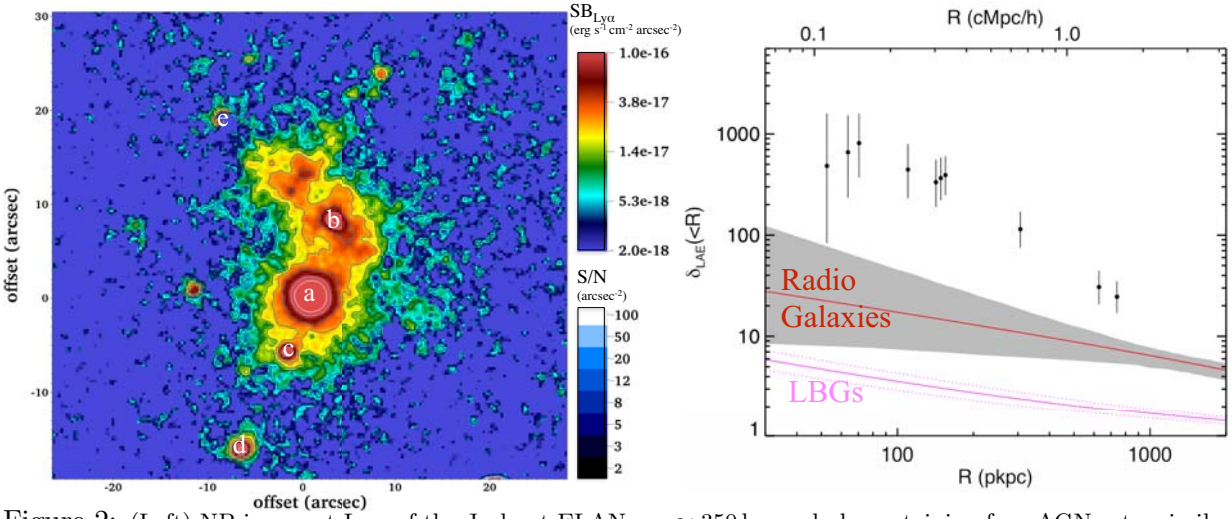

Figure 2: (Left) NB image at Lyα of the Jackpot ELAN, an $\approx 350\,$kpc nebula containing four AGNs at a similar redshift [marked a-d]. The field also shows a fifth quasar [e] which lies behind the nebula and provides an absorption spectrum of the gas. (Right) The data points indicate the cumulative overdensity profile of LAEs as a function of impact parameter R from the quasar SDSSJ0841+3921 [a]. The red and magenta curves respectively show the overdensity profile from a sample of high-z radio galaxies and LBGs around radio-quiet quasars (Trainor and Steidel, 2012). The overdensity around the Jackpot ELAN indicates it lies within a massive protocluster at $z = 2.2$. [Adapted from Hennawi et al. 2015]

2.2 The Jackpot ELAN

One reason the Slug's discovery came as a surprise was that we had previously searched in slit spectroscopy around $z \sim 2$ quasars for fluorescent emission and had largely failed (Hennawi and Prochaska, 2013). This search was motivated by a principal result of our QPQ survey that quasar halos exhibit a high covering fraction of optically thick gas (Prochaska et al., 2013b). If the quasar shines on this gas, $\approx 60\%$ of the ionizing photons are converted to Lyα at the surface. There was one obvious exception to the non-detections, the quasar SDSSJ0841+3921 which exhibited bright

Lyα emission to $\approx 150\,$kpc, which we then targeted with a NB filter on Keck/LRIS.

Figure 2 shows the Lyα image of this field and reveals the Jackpot ELAN (Hennawi et al., 2015), so-named because the data show 5 AGNs in $\approx 1'$! Four of these AGN (marked a-d) are at a coincident redshift – a 1 in $\approx 10^7$ chance occurrence even allowing for quasar clustering – and the fifth (marked e), is a background quasar that provides an absorption-line spectrum through the region. Similar to the Slug ELAN, we infer a very large cool gas mass from both the emission and absorption data. In addition, the absorption spectrum reveals a highly enriched medium and argues for a dense gas ($n_{\rm H} > 1\,{\rm cm}^{-3}$) in clumps with small characteristic sizes ($\approx 50\,$pc).

In contrast to the Slug, the field around the Jackpot ELAN exhibits a terrific overdensity of LAEs (Figure 2, right). Although our Lyα image only spans $\approx 3\,$cMpc, the region exhibits the hallmarks of a protocluster (Chiang et al., 2013). Indeed, the over-density in the central region rivals any previously reported. A key aspect of our program is to examine the physical association of these nebulae to protoclusters and thereby study the nascent, intracluster medium (ICM).

2.3 Other ELANe

At the time of this writing, we are aware of $\approx 10\,$ELANe discovered through a heterogeneous set of observing techniques. This includes the NB imaging of luminous quasars, follow-up Lyα imaging of candidate protoclusters (e.g. Cai et al., 2017a), and IFU observations with VLT/MUSE and Palomar/CWI (PIs are collaborators Cantalupo and Arrigoni-Battaia; Borisova et al., 2016a; Arrigoni-Battaia et al., 2017). Nearly all of the ELANe have been discovered by our collaboration and, as we describe next, we have on-going programs to dissect them. Already, there is a sufficiently large sample in-hand to address the primary science goals of this proposal. In addition, several large-sky surveys will yield even larger new samples. One project is the HETDEX survey which will discover Lyα nebulae at $z \approx 2-3.5$ across $\approx 400\,$sq. deg of the Northern sky. Another key project is the HyperSuprime Camera imaging survey on the Subaru telescope which includes a NB imaging component targeting Lyα emission at $z \sim 2$. In several respects, our program serves as a pathfinder for these and future large-sky surveys.

3 Astrophysics of the ELAN

In the following section (§ 4), we describe several scientific areas we will study using ELANe. To realize this science, but also as a complimentary science goal, a major thrust of our program is to dissect the ELAN phenomenon through a combination of follow-up observations and new theoretical modeling. This section describes our ongoing and planned activities.

3.1 Power Source(s)

Central to understanding the astrophysics of the ELANe is to establish the primary energy source(s) which powers their large Lyα luminosities, $L_{{\rm Ly}\alpha} > 10^{44}\,{\rm erg/s}$. These rival and even exceed the bolometric luminosity of an L^*, star-forming galaxy at $z \sim 2$. Because ELANe may be considered the extrema of LABs, one may first consider the mechanisms invoked to power those sources – gravitational infall (Faucher-Giguere et al., 2010), scattering of Lyα photons (Hayes et al., 2011), fluorescence of AGN ionizing radiation (Prescott et al., 2015). All of these processes may contribute to an ELAN. The physical scale and integrated luminosity of the ELANe, however, far exceed the models developed thus far for LABs. Additional astrophysical processes and/or multiple sources may be required, e.g. emission from multiple AGN, shocks from radio jets, thermal instability and hydrodynamic clumping from unstable 'shattering' (McCourt et al., 2016; Fielding et al., 2017b).

The principal challenge with distinguishing between these scenarios is that Lyα may be generated though multiple channels: via collisional excitation in shocked or cooling gas, as the final photon emitted in H recombination, via de-excitation following absorption of a Lyα photon. All of these may be relevant to the ELAN. Furthermore Lyα is a resonant line and cool gas is generally optically thick to this radiation, invoking important and complex radiative transfer (RT) effects (e.g. Cantalupo et al., 2005; Dijkstra et al., 2006). Yet another difficulty is that the driving source(s) may be hidden from our view. The majority of ELAN discovered thus far host at least one luminous AGN, but there are notable exceptions. For example, the MAMMOTH ELAN, with a luminosity of 2×10^{44} erg/s, shows only a very faint UV 'smudge' within it, yet, one suspects an obscured AGN (Cai et al., 2017b). These challenges motivate an observational program that brings additional diagnostics to bear on the problem: spatially resolved kinematics of the gas, polarization measurements of Lyα to constrain scattering scenarios, multi-wavelength spectroscopy to assess the ionization state and recombination rate of the gas, multi-wavelength imaging to search for and characterize embedded sources. Our program is executing all of these approaches to resolve the predominant astrophysical processes.

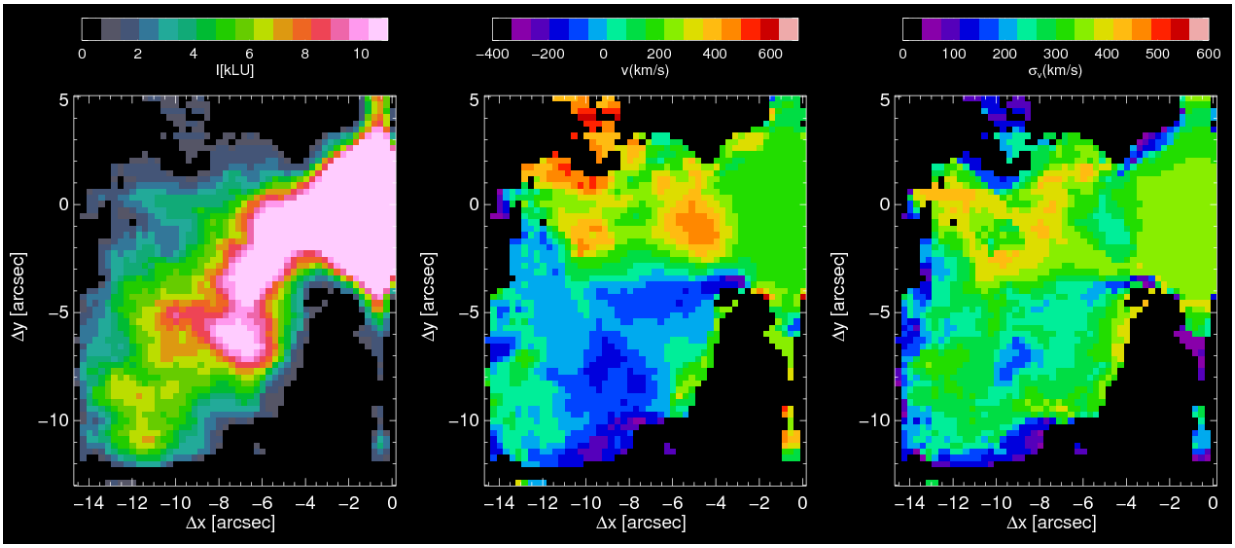

Figure 3: KCWI observations (4 hours in cloudy conditions) of the Slug nebulae. (left) Psuedo-narrow band image of the Lyα emission. (middle) velocity map relative to the CO redshift of the Slug quasar. (right) velocity dispersion map.

3.2 Kinematics

One path toward distinguishing between the various emission scenarios described above is to resolve the gas kinematics. Are the data indicative of non-gravitational motions, e.g. galactic-scale feedback? Are there multiple velocity components indicating multiple sources? Our investigation has begun using Lyα spectroscopy, primarily due to its high flux, although we recognize that RT effects can complicate the interpretation of this resonant line (e.g. Dijkstra and Kramer, 2012). We are proceeding cautiously and are constructing models with Lyα RT for direct comparison.

Figure 3 shows a recent KCWI IFU observation of the Slug ELAN obtained by Co-I C. Martin. The data reveal spatially compact, bright emission close to the central quasar (≈ 30 kpc in projection) and the diffuse nebula extending to ≈ 150 kpc. The spectrum also describes distinct kinematics for the two components. The central component is unresolved with a FWHM < 280km s^{-1} and a centroid consistent with the quasar's CO redshift. We detect this

component in several other spectral lines (e.g. He II 1640) and identify it as a distinct galaxy (see also, Martin et al., 2015). The nebula, in contrast, exhibits primarily blue-shifted emission with a larger velocity width (FWHM $\approx$ 450km s^{-1}). Neither emitting region shows the characteristic double-peak signature of simple Lyα RT through an optically thick medium. Altogether, the data imply two distinct emission mechanisms for the Slug: (1) a bright, compact source associated with a neighboring galaxy, possibly hosting its own AGN, and (2) the diffuse nebula characterized by relatively quiescent motions but offset from the central quasar by $\approx$ 1000km s^{-1}.

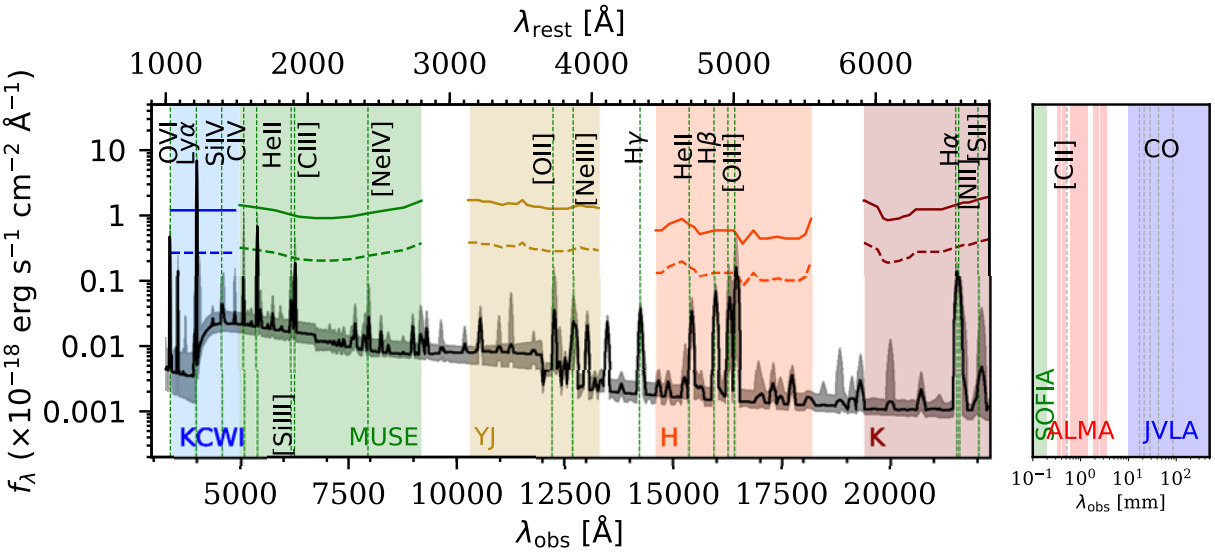

Figure 4: These panels describe the mulit-wavelength diagnostics that we are pursuing the analyze the ELANe. This includes IFU observations at optical wavelengths, near-IR spectroscopy, mid-IR photometry (SOFIA), and mm and radio interferometry (ALMA, JVLA). The spectrum is a model prediction for the Slug nebula. The solid curves at optical wavelengths show the 1σ and 3σ sensitivity limits for Keck/KCWI (approximate) and VLT/MUSE.

3.3 Multi-wavelength Analysis

Given the limitations and complications of interpreting H I Lyα observations alone (e.g. multiple excitation processes, RT effects), one is strongly motivated to examine the ELAN at other wavelengths. Such multi-wavelength data will further diagnose the astrophysics of the gas and will also reveal and assess additional central sources (e.g. obscured AGN). Figure 4 summarizes the range of diagnostics that we are pursuing with multi-wavelength campaigns on facilities ranging from large optical-IR telescopes (Keck, VLT), to the mid-IR (SOFIA), to the premier mm and radio interferometers (ALMA, JVLA) and sub-mm telescopes (APEX). The opportunities include: (1) Hα emission in the near-IR to constrain the fraction of Lyα emission generated by recombining gas. If Lyα is not strongly suppressed by RT effects, standard Case B recombination predicts a 8.7:1 flux ratio; (2) far-UV rest-frame emission from other nebular lines – He II 1640, C IV 1550. These appear in nebulae of radio galaxies (e.g. McCarthy, 1993) and generally signify a hard radiation field and/or shocked gas; (3) CO emission to search for associated molecular gas, e.g. in the outflows reported for low-z AGN (Veilleux et al., 2013); (4) mid-IR emission to reveal obscured AGN; (5) sub-mm emission to constrain dust and obscured star-formation.

Figure 5 shows examples of our multi-wavelength observations on the Slug and MAMMOTH ELAN: spectra at the Hα, He II, and C IV transitions. The Keck/MOSFIRE spectrum covering Hα emission from the Slug yields a tentative detection consistent with Case B recombination (Leibler et al., submitted). This implies that the Slug ELAN is powered primarily by the ionizing

flux of the central quasar. The non-detection of He II in the brightest part of the nebula (covered by the MOSFIRE slit) supports a clump model with number density $n_{\rm H} > 1\,{\rm cm}^{-3}$ (Cantalupo et al., in prep.). The additional line-emission from the MAMMOTH ELAN (Figure 5b), meanwhile, supports the interpretation of shocked gas accelerated by an obscured AGN (akin to radio galaxies). The strong detection of C IV indicates a highly enriched medium, perhaps approaching solar metallicity.

Maybe the most extraordinary follow-up observation of an ELAN has been the spatially-extended CO emission from the Spiderweb nebula by Collaborator Emonts (Figure 6; Emonts et al., 2016). The Spiderweb nebula, discovered first in Lyα, surrounds an aggregation of protocluster galaxies at $z \sim 2$. Low-surface-brightness observations of carbon-monoxide, CO(1-0), reveals a coincident, large reservoir of cold molecular gas. Most of this molecular gas lies between the protocluster galaxies and has low velocity dispersion, indicating that it is part of an enriched CGM. Its distribution follows that of diffuse UV-light from in situ star-formation that was detected with *HST* across the halo (Hatch et al., 2008). If one adopts a standard CO-H_2 conversion factor (only a guess given this highly unusual environment), the implied molecular mass is $M \approx 10^{11} M_\odot$! At first glance, this is truly astounding. On the other hand, we have argued from observations of other ELANe that the emission requires cool, dense clumps throughout the region with densities of at least $1\,{\rm cm}^{-3}$. It is plausible, if not inevitable, that a fraction of this gas will collapse to form a molecular medium. Our team has a wealth of additional data available to further study the multi-phase medium across the halo of the Spiderweb, including ALMA cycle-3 data of atomic CI(1-0) and molecular CO(4-3), scheduled VLA P-band observations to trace neutral hydrogen in 21cm absorption, and VLT/VIMOS IFU spectroscopy to further characterize the Lyα halo. If molecular halos like the one we see in the Spiderweb are common, they could present the predicted cold baryon cycle that drives the early growth of galaxies (e.g. Narayanan et al., 2015; Voit et al., 2015). We are pursuing similar observations with compact configurations at the Janksy Very Large Array (VLA17A-174, Priority A) on our newly discovered ELANe.

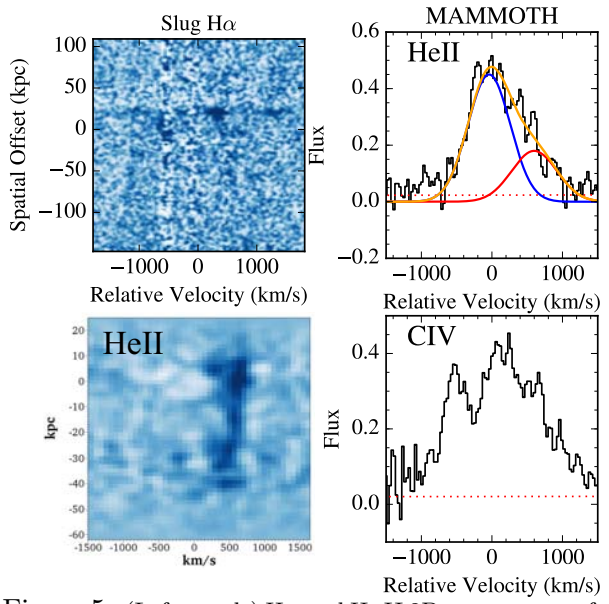

Figure 5: (Left panels) Hα and He II 2D spectroscopy for the Slug nebula from Keck/MOSFIRE and VLT/MUSE IFU observations. The tentative detection of Hα and correspondingly weak/absent He II emission implies radiation from a clumpy medium; (Right panels) He II and C IV spectroscopy of the inner region of the MAMMOTH ELAN. The line ratios are indicative of shocked gas and suggest an underlying obscured AGN (Cai et al., 2017b).

4 Science enabled by ELAN

Nearly independent of the underlying astrophysics driving ELAN emission, these phenomena offer a unique and powerful opportunity to examine several areas of scientific study: (1) the spatial distribution, kinematics, and enrichment of the cool halo gas surrounding massive galaxies; (2) the emission of ionizing radiation from luminous AGN – both apparent and obscured; (3) the formation of the proto-intracluster medium (proto-ICM).

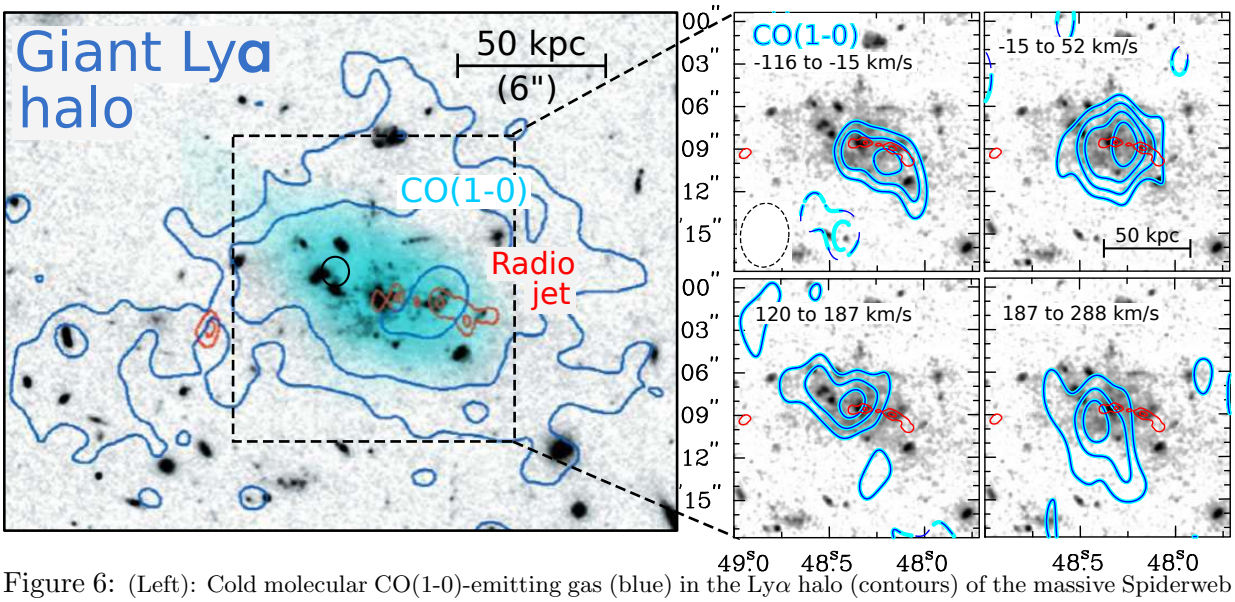

Figure 6: (Left): Cold molecular CO(1-0)-emitting gas (blue) in the Lyα halo (contours) of the massive Spiderweb nebula at $z \sim 2$. (Right): Velocity plots of the CO (contours; $-3, -2, 2, 3, 4, 5\sigma$). Most of the cold molecular gas lies in between proto-galaxies and has low velocity dispersion, indicating that it is the coldest phase of the inter-galactic medium. This cold gas fuels 'in-situ star-formation detected in the UV with HST/ACS across ~ 70 kpc (greyscale; Hatch+ 2008). It suggests that extended Lyα nebulae are truly multi-phase, and may fuel the early evolution of giant galaxies. [Adapted from Emonts et al. (2016)]

4.1 Illuminating the CGM

Over the past decade, the properties and origin of gaseous halos and the flows within them has been a forefront research topic. In large part, the intense activity was triggered by three advances: (i) a new theoretical paradigm that predicts the accretion of cool ($T \sim 10^4$ K) gas that flows into galaxies (e.g. Kereš et al., 2005; Dekel and Birnboim, 2006; Nelson et al., 2013); (ii) numerous dedicated surveys using bright background sources, primarily quasars, to sample the halo gas in absorption (e.g. Steidel et al., 2010; Prochaska et al., 2011; Tumlinson et al., 2011); and (iii) observational and theoretical evidence that galactic-scale winds are critical to galaxy formation (e.g. Weiner et al., 2009; Somerville and Davé, 2015; Rubin et al., 2014; Fielding et al., 2017b,a). The CGM experiments have confirmed early work that halos contain enriched gas (e.g. Lanzetta et al., 1995; Chen et al., 2001), and have statistically constrained the mass, metallicity and other properties of the medium.

At $z \sim 0$, for example, the COS-Halos survey has assessed the multi-phase CGM of L^* galaxies to derive a cool gas mass estimate $M \approx$ several $\times\, 10^{10} M_\odot$ with median metallicity of 1/3 solar, and similar estimates for a warm-hot phase traced by O VI (Tumlinson et al., 2011; Werk et al., 2014). At high z, where processes of galaxy formation are heightened (e.g. higher star formation rates), the CGM has been more sparsely sampled. It is more difficult to design and execute absorption-line experiments because the number of spectroscopically confirmed galaxies remains low, and these are isolated to select areas of the sky where there are few bright, background sources. Furthermore the IGM blankets many of the far-UV transitions that diagnose the CGM, imposing an additional systematic uncertainty on the analysis. Nevertheless, researchers have demonstrated a cool CGM surrounds the star-forming LBGs (Simcoe et al., 2006; Steidel et al., 2010; Rudie et al., 2012), the massive galaxies hosting quasars (Prochaska et al., 2013b), and the (presumably) lower mass halos hosting damped Lyα systems (Rubin et al., 2015). Amazingly, the sparse mass and metallicity estimates that exist also indicate a highly enriched gas and large

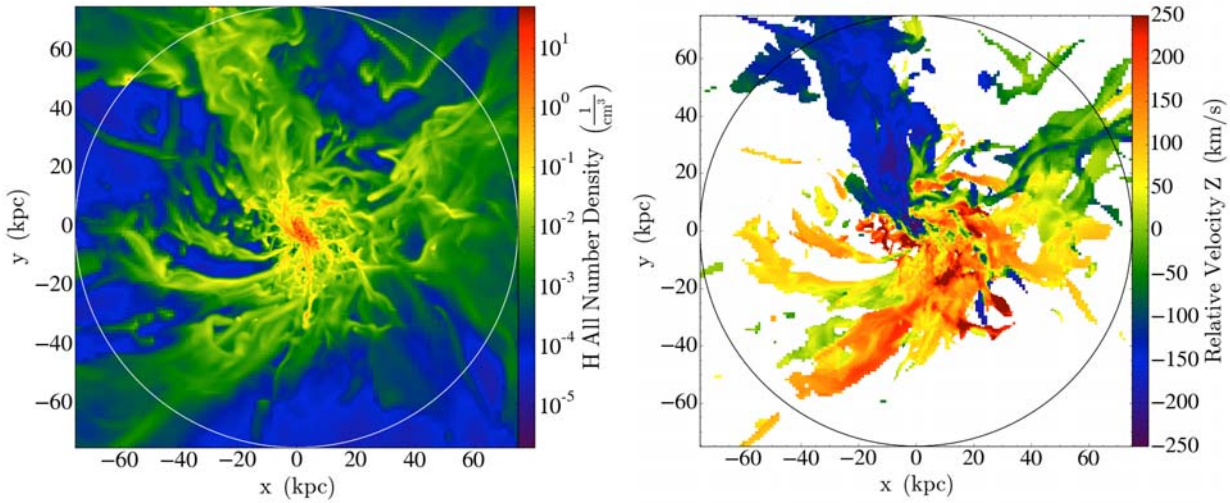

Figure 7: (left) Projected Hydrogen density map for gas accreting through a dark matter halo at $z = 3$ with a virial radius of 75 kpc (indicated by the circle). One notes the filament-like structures characteristic of the cold stream paradigm; (right) Line-of-sight velocity, mass-weighted and restricted to gas with $T < 10^5$ K and density $n_{\rm H} > 0.003\,{\rm cm}^{-3}$. As observed, the overall gas shows a net angular momentum due to the infalling motions of the streams. [Analysis performed by Collaborator Stewart]

mass ($\sim 10^{11} M_\odot$; Lehner et al., 2014; Crighton et al., 2015; Lau et al., 2016).

Although details of the cold stream paradigm are still under debate (e.g. Nelson et al., 2013), all of the models predict a reservoir of cool ($T \sim 10^4$K) gas embedded within a hot, diffuse and virialized plasma (e.g. Figure 7, left). Thus far, CGM experiments at $z \sim 2$ support this picture in that one detects a high incidence of cool gas in absorption (e.g. Rudie et al., 2012; Prochaska et al., 2013b). Figure 8 summarizes a key result of the QPQ survey: the incidence of optically thick hydrogen gas in the massive dark matter halos hosting quasars. Statistically, one observes a high incidence of such material to impact parameters of ≈ 150 kpc, approximately the virial radius of these halos. This high covering factor exceeds the basic predictions of the cold stream paradigm (Fumagalli et al., 2014), and feedback processes related to galactic-scale winds may be required to contribute (Faucher-Giguère et al., 2016).

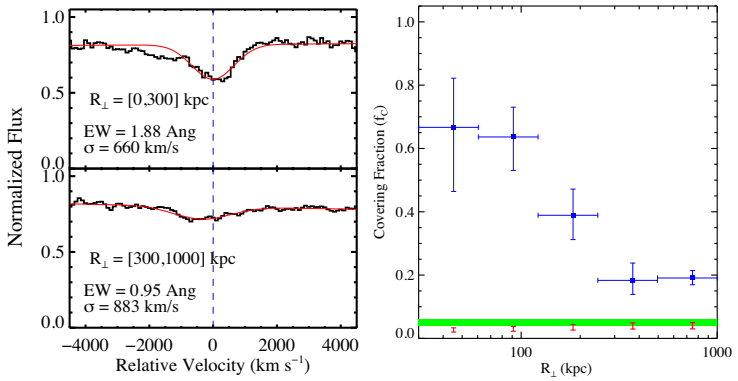

Figure 8: (Left) Average absorption in H I Lyα by gas in the halos and extended environment of $z \approx 2$ quasars (Prochaska et al., 2013a); (Right) Average covering fraction of optically thick gas in the same environment. Statistically, we recover a high incidence to ≈ 150 kpc far in excess of the random expectation (green band and red points).

Although the absorption-line experiment offers powerful constraints on the nature of halo gas, it has several inherent flaws. With absorption-line studies, one is limited to a statistical description of the gas; comparisons with the predicted gas distribution for individual galaxies (e.g. Figure 7) are essentially impossible. Furthermore, many of the key quantitative results are based on simple ionization models, stemming from reasonable assumptions about the gas, but this also reflects our ignorance of key aspects of its physical properties (e.g. temperature, density). It is now well-recognized, both empirically and theoretically, that one may also constrain the

CGM through emission-line observations (e.g. Lyα; Kollmeier et al., 2010). In principle, such data resolve the density, spatial distribution, and gas motions on scales of tens to hundreds kpc.

With our ELAN program, we will observe a large sample of individual dark matter halos at $z \sim 2-3$ for the analysis of CGM in emission. The nebulae shown throughout this proposal highlight our current progress at sensitively resolving the spatial distribution of cool gas to (at least) the virial radii of these halos. To zeroth order, these first results confirm the absorption-line results: we detect cool $T \sim 10^4$ K hydrogen gas to ≈ 150 kpc radius with a high covering fraction. In projection, the emission is generally asymmetric in distribution, especially as one extends to larger distances (Borisova et al., 2016a). The picture of narrow filaments feeding the central galaxy (e.g. Fumagalli et al., 2011) is not readily apparent, although we caution that a proper, quantitative comparison will require RT post-processing of hydrodynamic simulations.

Our collaboration has the expertise and computational resources for such quantitative comparison between data and theory, and we have published first results on the Slug ELAN (Cantalupo et al., 2014). A surprising result of this analysis is that one must impose an additional 'clumping factor' in the hydrodynamic solutions to even qualitatively reproduce the observed morphology and luminosity of the Lyα emission. This implies hydrodynamic processes on sub-kpc scales that are not captured by even zoom-in simulations, e.g. pressure-induced 'shattering' of cool gas (McCourt et al., 2016; Fielding et al., 2017b). This model inference of dense, unresolved clumps is supported by analysis of other nebular lines of the Slug (Arrigoni Battaia et al., 2015) and the remarkable detection of CO gas in the Spiderweb nebula (Figure 6).

With even a modest sample of well-studied ELANe, we will gain tremendous new insight into the properties of the $z \sim 2$ CGM. We will combine these measurements with the observational constraints imposed by absorption-line experiments to comprehensively describe the CGM. Furthermore, our collaboration is extending CGM studies to the dark matter halos hosting sub-mm galaxies (Fu et al., 2016) and damped Lyα systems (Rubin et al., 2015) in absorption and emission Fumagalli et al. (2017). This work is already inspiring new models and treatments of hydrodynamics in galaxy halos, and has the potential to transform the paradigm of gas accretion.

In addition to the spatial distribution and density of the cool CGM, the cold stream paradigm makes clear predictions on the gas kinematics. First, the streams infall with characteristic speeds of ~ 100km s^{-1}, roughly independent of the halo mass. At this modest velocity, hydrodynamic instabilities do not completely disrupt the gas nor do shocks heat it far beyond 10^4 K. Second, the infalling gas frequently exhibits a net angular momentum that drives galaxy rotation (e.g. Stewart et al., 2011; Danovich et al., 2015). An example of the predicted gas kinematics of infalling gas within a $z \sim 3$ dark matter halo is illustrated in Figure 7. With the ELAN, we can directly test these hypotheses. This may be pursued with Lyα kinematics, which are the most sensitive probe of the gas to large spatial scales and through optically-thin lines (e.g. He II 1640) when detected. The observational requirement is spatially resolved kinematics across a several hundred kpc field-of-view; our program is leveraging new IFU instruments on 10-m class telescopes for this purpose. Figure 9 shows three views of the Fabulous ELAN observed with VLT/MUSE Arrigoni Battaia et al. (2017). The left panel shows a pseudo-NB image at Lyα constructed from the data cube which reveals nebular emission extending ≈ 300 kpc across and several Lyα-emitting point sources including the targeted quasar SDSS J1020+1040. Similar to several other ELAN, the environment is over-abundant with AGN.

The right panel of Figure 9 shows the flux-weighted centroid of the Lyα emission throughout the ELAN. The ELAN exhibits a substantial velocity shear as one progresses from its SE edge to the NW. The lower half of the ELAN shows systematically lower velocities (by ≈ 250km s^{-1})

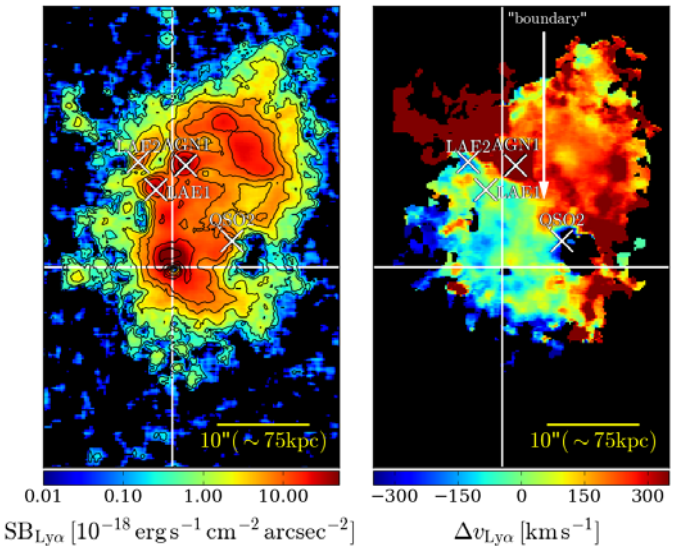

Figure 9: The enormous Lyα nebula surrounding the quasar J1020+1040. (Left) "optimally-extracted" Lyα surface brightness map obtained after subtraction of the quasar PSF and continuum in the final MUSE datacube. The image reveals an extremely bright nebula extending several hundred kpc on the North-west side of the quasar. Four Lyα emitters (small diagonal crosses) are associated with the quasar, and the ELAN. (Right) flux-weighted velocity-shift map with respect to the systemic redshift of the quasar. A large-scale rotation-like pattern is evident, whose transition region is referred to as "boundary". In each panel the large white cross indicates the position of the targeted quasar. [Adapted from Arrigoni Battaia et al. (2017)]

than the upper half and there is a relatively sharp discontinuity across the 'boundary'. The flux-weighted standard deviation is low ($\sigma_v \approx 200\,\mathrm{km\ s^{-1}}$), nearly consistent with the spectral resolution of MUSE. The motions within this ELAN are highly coherent and support the signatures of infall characteristic of the simulations. Our program will obtain deep kinematic maps of a large sample of ELANe with VLT/MUSE (Collaborators Cantalupo, Arrigoni-Battaia) and Keck/KCWI to examine the diversity of gas kinematics within the CGM of $z \sim 2-3$ galaxies.

4.2 Constraining the Emission of Quasar Ionizing Radiation

The unified model for AGN emission synthesizes the UV luminous sources termed Type I quasars with the obscured Type-2 sources by invoking a dust-obscuring torus that surrounds the accreting black hole. Over the past decade, significant progress has been made in identifying sizable samples of obscured quasars, aka Type-2 QSOs, from mid-IR, X-ray, and the SDSS spectroscopic survey (e.g. Zakamska et al., 2003; Stern et al., 2005; Reyes et al., 2008; Alexandroff et al., 2013). However, the vast majority of these are low-luminosity objects at $z < 1$, whereas only handfuls of bonafide Type-2 QSOs are known at $z \sim 2$ with bolometric luminosities $L_{\rm bol} \gtrsim 10^{46}\,\mathrm{erg\,s^{-1}}$ ($M_{\rm B} < -23$), i.e. comparable to the typical luminosity of Type-1 QSOs. Decades of work on QSO demographics have clearly established that the Type-1 QSO luminosity density peaks at $z \sim 2.5$. Thus, the conspicuous lack of luminous Type-2 QSOs at $z \sim 2$ suggests, contrary to AGN unification, that the obscuring medium is quenched or has lower covering factor at high luminosities (Hasinger, 2008). If true this would have profound implications for AGN physics. Indeed the *receding torus* model (Lawrence, 1991) postulates exactly this behavior because of dust sublimation, whereas models that equate the torus to a hydrodynamic disk-driven outflow make similar predictions (Konigl and Kartje, 1994; Elitzur and Shlosman, 2006). Alternatively, luminous high-z Type-2 QSOs may have simply eluded discovery. To date, X-ray and mid-IR telescopes have surveyed very small areas $\sim 1\,\mathrm{deg^2}$, and thus lack the volume to identify rare, bright Type-2s.

Results from absorption-line analysis support this scenario for the anisotropic emission of ionizing radiation from luminous AGN. The high incidence of optically thick gas in the transverse dimension described by Figure 8, for example, strongly contrasts with the very low incidence of Lyman limits at the quasar redshift (Hennawi and Prochaska, 2007; Prochaska et al., 2013a). Statistically, our results imply anisotropic emission with an opening angle $\Omega \lesssim 2\pi$ (Hennawi and

Prochaska, 2013), consistent with AGN unification models and best estimates for the fraction of obscured quasars (e.g. Lacy et al., 2004). With our QPQ program, we have extended the analysis to several cMpc (Prochaska et al., 2013a) and are currently studying the transverse proximity effect (TPE) in optically thin gas at these larger separations. The TPE absorption-line analysis will further constrain the lifetime and geometry of quasar emission.

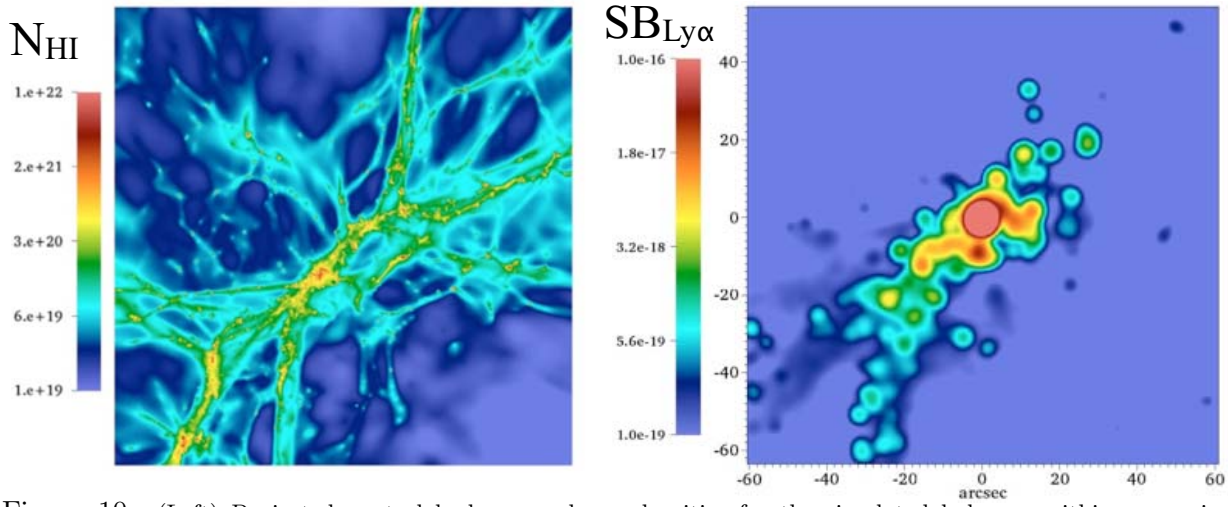

Figure 10: (Left) Projected neutral hydrogen column densities for the simulated halo gas within a massive halo at $z \approx 2$. (Right) Predicted Lyα surface brightness resulting from an embedded, luminous quasar with an opening angle $\Omega = 2\pi$, oriented towards the observer. The calculation includes RT post-processing to account for photoionization, Lyα fluorescence, and Lyα scattering (Cantalupo et al., 2014).

With the proposed ELAN project, we will perform new analysis to include constraints from observations of Lyα emission. The analysis can and will include all of the Lyα data of our survey, i.e. sensitive non-detections, the faint nebulae that characterize the majority of the sample, and the luminous ELAN. Statistically, these describe the average coupling of the quasar ionizing flux to the surrounding CGM. This analysis will require modeling of the cool CGM and RT treatments of the quasar's ionizing flux and the emergent Lyα emission. Collaborator Cantalupo has developed the RADAMESH package especially for this purpose, and Figure 10 shows maps generated to model the Slug. We will generate a suite of models with varying scenarios on the quasar emission, e.g. emission geometry, opening angles, quasar lifetimes. The constraints from the ~ 100 kpc scales probed by Lyα emission will be combined with the TPE at Mpc scales to statistically describe the emission from $z \sim 2$ AGN. In turn, this analysis informs AGN demographics, the impact of radiative feedback on galaxy halos, and the morphology of reionization.

We further note that our program will provide two additional observational constraints on quasar emission. We have obtained deep NB imaging at Lyα in approximately 10 fields around luminous quasars to search for galaxies fluorescently illuminated by AGN (e.g. Cantalupo et al., 2012). The incidence and spatial distribution of these sources relate to the quasar lifetime and opening angle of quasar emission (Cantalupo et al., 2012; Trainor and Steidel, 2013; Borisova et al., 2016b). Lastly, polarization measurements obtained with the Keck/LRIS polarimeter (in-hand for the Slug nebula) and KCWI reveal the spatial distribution of scattered Lyα photons from the central sources, an independent constraint on the emission models.

4.3 ELANe and Protoclusters

Shortly after the discovery of one of the first high-z protoclusters SSA22, observers identified a remarkable incidence of Lyα nebulae throughout the structure (Steidel et al., 2000; Matsuda

et al., 2004). A close link between the two phenomena is now established (e.g. Matsuda et al., 2011), and the ELANe appear to participate. Several of the ELANe described here – the Jackpot, MAMMOTH, and Spiderweb nebulae – all reside in extreme overdensities characteristic of a protocluster. Presently, the association is only correlative, but we have speculated that the physical conditions and processes within protoclusters are highly conducive to ELANe (e.g. higher gas density, elevated AGN activity, accelerated gas accretion and star-formation; Hennawi et al., 2015). In the proposed program, we will further examine this link and leverage ELAN to examine processes of protocluster assembly.

Our collaboration is actively searching for new ELAN in $z \sim 2$ candidate protoclusters with follow-up NB imaging at Lyα (e.g. Cai et al., 2017a). This includes an ongoing program with the HyperSuprime Camera (HSC) on Subaru (PI Prochaska) which has an optimal field-of-view and high sensitivity. We have additional programs on smaller aperture facitilies (e.g. KPNO 4m; PI Cai) and we will perform targeted IFU observations in the densest regions of confirmed protoclusters. Our goal is to survey several tens of $z \sim 2$ protoclusters in the next several years to statistically establish the incidence and distribution of Lyα nebulae within these structures.

The ELANe discovered within protoclusters, meanwhile, provide unique insight into cluster formation. On the smallest scales (~ 100 kpc), we may search for evidence of enhanced galaxy formation activity as evident in the Spiderweb protocluster (Figure 6). These data reveal the assembly history of brightest cluster galaxies. On the largest scale of ELANe (≈ 2 cMpc), our observations describe the heating and enrichment of the proto-ICM. For these systems especially, we will obtain deep IFU spectroscopy at the O VI and N V transitions which probe gas at $T \sim 10^{5-6}$ K. This gas may interface between the cool medium emitting Lyα and a nascent, hot ICM. Lastly, the ELANe reveal aspects of AGN feedback on the proto-ICM, in progress. This includes both radiation feedback which heats the medium and constraints on kinetic feedback in the dynamics of the gas around luminous and obscured AGN (e.g. Figure 3). With the era of large-sky surveys with 10 m-class telescopes upon us (e.g. HSC, HETDEX), research on protoclusters will transition from several sources to statistical samples. Our program will greatly complement such projects and motivate additional follow-up observations.

5 Broader Impact

The scientific projects of our ELAN program, described in the preceding sections, address several of the most active areas of research in the high-z universe: studies of massive galaxy formation, AGN physics, and protocluster assembly. Our program uniquely complements a wealth of other observational studies, especially large-area imaging and spectroscopic surveys.

The datasets we are acquiring on the ELANe include deep NB and broad-band optical imaging, slit and IFU spectroscopy at optical and near-IR wavelengths, optical polarimetry at Lyα, and mm and radio interferometric and sub-mm single-dish observations. While our focus is on the ELANe, these data will enable new investigations by our team and additional collaborators on topics including: (1) correlations between ELANe properties and those of coincident and neighboring galaxies. Such associations bear on the processes of galaxy formation in dense environments; (2) the physical association of galaxies to absorption-line systems (e.g. metal-line systems like Mg II, C IV). The IFU datasets, in particular, are extremely valuable for this science, and many of the quasars targeted for ELANe have or will have high quality absorption-line spectra; (3) new, deep surveys for LAEs at $z \sim 2-3$; (4) astrophysical analysis of the so-called 'dark' galaxies, those illuminated fluorescently by quasar ionizing radiation (Cantalupo et al., 2014); and (5) the discovery and analysis of a large new sample of modest-sized LABs. All of our deep

References

Alexandroff, R., M. A. Strauss, J. E. Greene, N. L. Zakamska, N. P. Ross, W. N. Brandt, G. Liu, P. S. Smith, J. Ge, F. Hamann, A. D. Myers, P. Petitjean, D. P. Schneider, H. Yesuf, and D. G. York, 2013: Candidate type II quasars at $2 < z < 4.3$ in the Sloan Digital Sky Survey III. *MNRAS*, **435**, 3306–3325.

Arrigoni-Battaia, F., S. Cantalupo, J. F. Hennawi, and J. X. Prochaska, 2017: Blobs. *Science*, submitted.

Arrigoni Battaia, F., J. F. Hennawi, J. X. Prochaska, and S. Cantalupo, 2015: Deep He II and C IV Spectroscopy of a Giant Lyα Nebula: Dense Compact Gas Clumps in the Circumgalactic Medium of a z ˜ 2 Quasar. *ApJ*, **809**, 163.

Arrigoni Battaia, F., J. X. Prochaska, J. F. Hennawi, A. Obreja, T. Buck, S. Cantalupo, A. A. Dutton, and A. V. Macciò, 2017: Inspiraling Halo Accretion Mapped in Lyman-α Emission around a $z \sim 3$ Quasar. *ArXiv e-prints*.

Borisova, E., S. Cantalupo, S. J. Lilly, R. A. Marino, S. G. Gallego, R. Bacon, J. Blaizot, N. Bouché, J. Brinchmann, C. M. Carollo, J. Caruana, H. Finley, E. C. Herenz, J. Richard, J. Schaye, L. A. Straka, M. L. Turner, T. Urrutia, A. Verhamme, and L. Wisotzki, 2016a: Ubiquitous Giant Lyα Nebulae around the Brightest Quasars at $z \sim 3.5$ Revealed with MUSE. *ApJ*, **831**, 39.

Borisova, E., S. J. Lilly, S. Cantalupo, J. X. Prochaska, O. Rakic, and G. Worseck, 2016b: Constraining the Lifetime and Opening Angle of Quasars using Fluorescent Lyman α Emission: The Case of Q0420-388. *ApJ*, **830**, 120.

Cai, Z., X. Fan, F. Bian, A. Zabludoff, Y. Yang, J. X. Prochaska, I. McGreer, Z.-Y. Zheng, N. Kashikawa, R. Wang, B. Frye, R. Green, and L. Jiang, 2017a: Mapping the Most Massive Overdensities through Hydrogen (MAMMOTH). II. Discovery of the Extremely Massive Overdensity BOSS1441 at $z = 2.32$. *ApJ*, **839**, 131.

Cai, Z., X. Fan, Y. Yang, F. Bian, J. X. Prochaska, A. Zabludoff, I. McGreer, Z.-Y. Zheng, R. Green, S. Cantalupo, B. Frye, E. Hamden, L. Jiang, N. Kashikawa, and R. Wang, 2017b: Discovery of an Enormous Lyα Nebula in a Massive Galaxy Overdensity at z = 2.3. *ApJ*, **837**, 71.

Cantalupo, S., F. Arrigoni-Battaia, J. X. Prochaska, J. F. Hennawi, and P. Madau, 2014: A cosmic web filament revealed in Lyman-α emission around a luminous high-redshift quasar. *Nature*, **506**, 63–66.

Cantalupo, S., S. J. Lilly, and M. G. Haehnelt, 2012: Detection of dark galaxies and circumgalactic filaments fluorescently illuminated by a quasar at z = 2.4. *MNRAS*, **425**, 1992–2014.

Cantalupo, S., C. Porciani, S. J. Lilly, and F. Miniati, 2005: Fluorescent Lyα Emission from the High-Redshift Intergalactic Medium. *ApJ*, **628**, 61–75.

Chen, H.-W., K. M. Lanzetta, and J. K. Webb, 2001: The Origin of C IV Absorption Systems at Redshifts $z < 1$: Discovery of Extended C IV Envelopes around Galaxies. *ApJ*, **556**, 158–163.

Chiang, Y.-K., R. Overzier, and K. Gebhardt, 2013: Ancient Light from Young Cosmic Cities: Physical and Observational Signatures of Galaxy Proto-clusters. *ApJ*, **779**, 127.

Crighton, N. H. M., J. F. Hennawi, R. A. Simcoe, K. L. Cooksey, M. T. Murphy, M. Fumagalli, J. X. Prochaska, and T. Shanks, 2015: Metal-enriched, subkiloparsec gas clumps in the circumgalactic medium of a faint z = 2.5 galaxy. *MNRAS*, **446**, 18–37.

Danovich, M., A. Dekel, O. Hahn, D. Ceverino, and J. Primack, 2015: Four phases of angular-momentum buildup in high-z galaxies: from cosmic-web streams through an extended ring to disc and bulge. *MNRAS*, **449**, 2087–2111.

Dekel, A. and Y. Birnboim, 2006: Galaxy bimodality due to cold flows and shock heating. *MNRAS*, **368**, 2–20.

Dijkstra, M., Z. Haiman, and M. Spaans, 2006: Lyα Radiation from Collapsing Protogalaxies. I. Characteristics of the Emergent Spectrum. *ApJ*, **649**, 14–36.

Dijkstra, M. and R. Kramer, 2012: Line transfer through clumpy, large-scale outflows: Ly α absorption and haloes around star-forming galaxies. *MNRAS*, **424**, 1672–1693.

Elitzur, M. and I. Shlosman, 2006: The AGN-obscuring Torus: The End of the "Doughnut" Paradigm? *ApJL*, **648**, L101–L104.

Emonts, B., M. D. Lehnert, M. Villar-Martin, R. P. Norris, and R. D. Ekers, 2016: Molecular Gas in the Halo Fuels the Growth of a Massive Cluster Galaxy at High Redshift. *Science*, in press.

Faucher-Giguere, C., D. Keres, M. Dijkstra, L. Hernquist, and M. Zaldarriaga, 2010: Lyman-alpha Cooling Emission from Galaxy Formation. *ArXiv e-prints*.

Faucher-Giguère, C.-A., R. Feldmann, E. Quataert, D. Kereš, P. F. Hopkins, and N. Murray, 2016: A stellar feedback origin for neutral hydrogen in high-redshift quasar-mass haloes. *MNRAS*, **461**, L32–L36.

Fielding, D., E. Quataert, D. Martizzi, and C.-A. Faucher-Giguère, 2017a: How supernovae launch galactic winds? *MNRAS*, **470**, L39–L43.

Fielding, D., E. Quataert, M. McCourt, and T. A. Thompson, 2017b: The impact of star formation feedback on the circumgalactic medium. *MNRAS*, **466**, 3810–3826.

Fu, H., J. F. Hennawi, J. X. Prochaska, R. Mutel, C. Casey, A. Cooray, D. Kereš, Z.-Y. Zhang, D. Clements, J. Isbell, C. Lang, D. McGinnis, M. J. Michalowski, K. Mooley, D. Perley, A. Stockton, and D. Thompson, 2016: The Circumgalactic Medium of Submillimeter Galaxies. I. First Results from a Radio-identified Sample. *ApJ*, **832**, 52.

Fumagalli, M., J. F. Hennawi, J. X. Prochaska, D. Kasen, A. Dekel, D. Ceverino, and J. Primack, 2014: Confronting Simulations of Optically Thick Gas in Massive Halos with Observations at z = 2-3. *ApJ*, **780**, 74.

Fumagalli, M., R. Mackenzie, J. Trayford, T. Theuns, S. Cantalupo, L. Christensen, J. P. U. Fynbo, P. Møller, J. O'Meara, J. X. Prochaska, M. Rafelski, and T. Shanks, 2017: Witnessing galaxy assembly in an extended $z \approx 3$ structure. *MNRAS*, **471**, 3686–3698.

Fumagalli, M., J. X. Prochaska, D. Kasen, A. Dekel, D. Ceverino, and J. R. Primack, 2011: Absorption-line systems in simulated galaxies fed by cold streams. *MNRAS*, **418**, 1796–1821.

Hasinger, G., 2008: Absorption properties and evolution of active galactic nuclei. *A & A*, **490**, 905–922.

Hatch, N. A., R. A. Overzier, H. J. A. Röttgering, J. D. Kurk, and G. K. Miley, 2008: Diffuse UV light associated with the Spiderweb Galaxy: evidence for in situ star formation outside galaxies. *MNRAS*, **383**, 931–942.

Hayes, M., C. Scarlata, and B. Siana, 2011: Central powering of the largest Lyman-α nebula is revealed by polarized radiation. *Nature*, **476**, 304–307.

Heckman, T. M., G. K. Miley, M. D. Lehnert, and W. van Breugel, 1991: Spatially resolved optical images of high-redshift quasi-stellar objects. *ApJ*, **370**, 78–101.

Hennawi, J. F. and J. X. Prochaska, 2007: Quasars Probing Quasars. II. The Anisotropic Clustering of Optically Thick Absorbers around Quasars. *ApJ*, **655**, 735–748 (QPQ2).

—, 2013: Quasars Probing Quasars. IV. Joint Constraints on the Circumgalactic Medium from Absorption and Emission. *ApJ*, **766**, 58 (QPQ4).

Hennawi, J. F., J. X. Prochaska, S. Burles, M. A. Strauss, G. T. Richards, D. J. Schlegel, X. Fan, D. P. Schneider, N. L. Zakamska, M. Oguri, J. E. Gunn, R. H. Lupton, and J. Brinkmann, 2006: Quasars Probing Quasars. I. Optically Thick Absorbers near Luminous Quasars. *ApJ*, **651**, 61–83 (QPQ1).

Hennawi, J. F., J. X. Prochaska, S. Cantalupo, and F. Arrigoni-Battaia, 2015: Quasar quartet embedded in giant nebula reveals rare massive structure in distant universe. *Science*, **348**, 779–783.

Kereš, D., N. Katz, D. H. Weinberg, and R. Davé, 2005: How do galaxies get their gas? *MNRAS*, **363**, 2–28.

Kollmeier, J. A., Z. Zheng, R. Davé, A. Gould, N. Katz, J. Miralda-Escudé, and D. H. Weinberg, 2010: Lyα Emission from Cosmic Structure. I. Fluorescence. *ApJ*, **708**, 1048–1075.

Konigl, A. and J. F. Kartje, 1994: Disk-driven hydromagnetic winds as a key ingredient of active galactic nuclei unification schemes. *ApJ*, **434**, 446–467.

Lacy, M., L. J. Storrie-Lombardi, A. Sajina, P. N. Appleton, L. Armus, S. C. Chapman, P. I. Choi, D. Fadda, F. Fang, D. T. Frayer, I. Heinrichsen, G. Helou, M. Im, F. R. Marleau, F. Masci, D. L. Shupe, B. T. Soifer, J. Surace, H. I. Teplitz, G. Wilson, and L. Yan, 2004: Obscured and Unobscured Active Galactic Nuclei in the Spitzer Space Telescope First Look Survey. *ApJS*, **154**, 166–169.

Lanzetta, K. M., D. V. Bowen, D. Tytler, and J. K. Webb, 1995: The gaseous extent of galaxies and the origin of Lyman-alpha absorption systems: A survey of galaxies in the fields of Hubble Space Telescope spectroscopic target QSOs. *ApJ*, **442**, 538–568.

Lau, M. W., J. X. Prochaska, and J. F. Hennawi, 2016: Quasars Probing Quasars. VIII. The Physical Properties of the Cool Circumgalactic Medium Surrounding z ˜ 2-3 Massive Galaxies Hosting Quasars. *ApJS*, **226**, 25.

Lawrence, A., 1991: The relative frequency of broad-lined and narrow-lined active galactic nuclei - Implications for unified schemes. *MNRAS*, **252**, 586–592.

Lehner, N., J. M. O'Meara, A. J. Fox, J. C. Howk, J. X. Prochaska, V. Burns, and A. A. Armstrong, 2014: Galactic and Circumgalactic O VI and its Impact on the Cosmological Metal and Baryon Budgets at $2 < z <\tilde{} 3.5$. *ApJ*, **788**, 119.

Martin, D. C., M. Matuszewski, P. Morrissey, J. D. Neill, A. Moore, S. Cantalupo, J. X. Prochaska, and D. Chang, 2015: A giant protogalactic disk linked to the cosmic web. *Nature*, **524**, 192–195.

Matsuda, Y., T. Yamada, T. Hayashino, H. Tamura, R. Yamauchi, M. Ajiki, S. S. Fujita, T. Murayama, T. Nagao, K. Ohta, S. Okamura, M. Ouchi, K. Shimasaku, Y. Shioya, and Y. Taniguchi, 2004: A Subaru Search for Lyα Blobs in and around the Protocluster Region At Redshift z = 3.1. *AJ*, **128**, 569–584.

Matsuda, Y., T. Yamada, T. Hayashino, R. Yamauchi, Y. Nakamura, N. Morimoto, M. Ouchi, Y. Ono, K. Kousai, E. Nakamura, M. Horie, T. Fujii, M. Umemura, and M. Mori, 2011: The Subaru Lyα blob survey: a sample of 100-kpc Lyα blobs at z= 3. *MNRAS*, **410**, L13–L17.

McCarthy, P. J., 1993: High redshift radio galaxies. *ARAA*, **31**, 639–688.

McCourt, M., S. P. Oh, R. M. O'Leary, and A.-M. Madigan, 2016: A Characteristic Scale for Cold Gas. *ArXiv e-prints*.

Morrissey, P., M. Matuszewski, C. Martin, A. Moore, S. Adkins, H. Epps, R. Bartos, J. Cabak, D. Cowley, J. Davis, A. Delacroix, J. Fucik, D. Hilliard, E. James, S. Kaye, N. Lingner, J. D. Neill, C. Pistor, D. Phillips, C. Rockosi, and B. Weber, 2012: The Keck Cosmic Web Imager: a capable new integral field spectrograph for the W. M. Keck Observatory. In *Ground-based and Airborne Instrumentation for Astronomy IV*, vol. 8446 of *SPIE*, p. 844613.

Narayanan, D., M. Turk, R. Feldmann, T. Robitaille, P. Hopkins, R. Thompson, C. Hayward, D. Ball, C.-A. Faucher-Giguère, and D. Kereš, 2015: The formation of submillimetre-bright galaxies from gas infall over a billion years. *Nature*, **525**, 496–499.

Nelson, D., M. Vogelsberger, S. Genel, D. Sijacki, D. Kereš, V. Springel, and L. Hernquist, 2013: Moving mesh cosmology: tracing cosmological gas accretion. *MNRAS*, **429**, 3353–3370.

Prescott, M. K. M., I. Momcheva, G. B. Brammer, J. P. U. Fynbo, and P. Møller, 2015: Overturning the Case for Gravitational Powering in the Prototypical Cooling Lyα Nebula. *ApJ*, **802**, 32.

Prochaska, J. X., J. F. Hennawi, K.-G. Lee, S. Cantalupo, J. Bovy, S. G. Djorgovski, S. L. Ellison, M. Wingyee Lau, C. L. Martin, A. Myers, K. H. R. Rubin, and R. A. Simcoe, 2013a: Quasars Probing Quasars. VI. Excess H I Absorption within One Proper Mpc of z ˜ 2 Quasars. *ApJ*, **776**, 136.

Prochaska, J. X., J. F. Hennawi, and R. A. Simcoe, 2013b: A Substantial Mass of Cool, Metal-enriched Gas Surrounding the Progenitors of Modern-day Ellipticals. *ApJL*, **762**, L19 (QPQ5).

Prochaska, J. X., M. W. Lau, and J. F. Hennawi, 2014: Quasars Probing Quasars. VII. The Pinnacle of the Cool Circumgalactic Medium Surrounds Massive z ˜ 2 Galaxies. *ApJ*, **796**, 140.

Prochaska, J. X., J. M. O'Meara, M. Fumagalli, R. A. Bernstein, and S. M. Burles, 2015: The Keck + Magellan Survey for Lyman Limit Absorption. III. Sample Definition and Column Density Measurements. *ApJS*, **221**, 2.

Prochaska, J. X., B. Weiner, H.-W. Chen, J. Mulchaey, and K. Cooksey, 2011: Probing the Intergalactic Medium/Galaxy Connection. V. On the Origin of Lyα and O VI Absorption at $z < 0.2$. *ApJ*, **740**, 91.

Prochaska, J. X., A. M. Wolfe, J. C. Howk, E. Gawiser, S. M. Burles, and J. Cooke, 2007: The UCSD/Keck Damped Lyα Abundance Database: A Decade of High-Resolution Spectroscopy. *ApJS*, **171**, 29–60.

Reyes, R., N. L. Zakamska, M. A. Strauss, J. Green, J. H. Krolik, Y. Shen, G. T. Richards, S. F. Anderson, and D. P. Schneider, 2008: Space Density of Optically Selected Type 2 Quasars. *AJ*, **136**, 2373–2390.

Rubin, K. H. R., J. F. Hennawi, J. X. Prochaska, R. A. Simcoe, A. Myers, and M. W. Lau, 2015: Dissecting the Gaseous Halos of $z\sim2$ Damped Lyα Systems with Close Quasar Pairs. *ApJ*, **808**, 38.

Rubin, K. H. R., J. X. Prochaska, D. C. Koo, A. C. Phillips, C. L. Martin, and L. O. Winstrom, 2014: Evidence for Ubiquitous Collimated Galactic-scale Outflows along the Star-forming Sequence at z ˜ 0.5. *ApJ*, **794**, 156.

Rudie, G. C., C. C. Steidel, R. F. Trainor, O. Rakic, M. Bogosavljević, M. Pettini, N. Reddy, A. E. Shapley, D. K. Erb, and D. R. Law, 2012: The Gaseous Environment of High-z Galaxies: Precision Measurements of Neutral Hydrogen in the Circumgalactic Medium of z ˜ 2-3 Galaxies in the Keck Baryonic Structure Survey. *ApJ*, **750**, 67.

Simcoe, R. A., W. L. W. Sargent, M. Rauch, and G. Becker, 2006: Observations of Chemically Enriched QSO Absorbers near z˜2.3 Galaxies: Galaxy Formation Feedback Signatures in the Intergalactic Medium. *ApJ*, **637**, 648–668.

Somerville, R. S. and R. Davé, 2015: Physical Models of Galaxy Formation in a Cosmological Framework. *ARAA*, **53**, 51–113.

Steidel, C. C., K. L. Adelberger, A. E. Shapley, M. Pettini, M. Dickinson, and M. Giavalisco, 2000: Lyα Imaging of a Proto-Cluster Region at $z = 3.09$. *ApJ*, **532**, 170–182.

Steidel, C. C., D. K. Erb, A. E. Shapley, M. Pettini, N. Reddy, M. Bogosavljević, G. C. Rudie, and O. Rakic, 2010: The Structure and Kinematics of the Circumgalactic Medium from Far-ultraviolet Spectra of z ˜= 2-3 Galaxies. *ApJ*, **717**, 289–322.

Stern, D., P. Eisenhardt, V. Gorjian, C. S. Kochanek, N. Caldwell, D. Eisenstein, M. Brodwin, M. J. I. Brown, R. Cool, A. Dey, P. Green, B. T. Jannuzi, S. S. Murray, M. A. Pahre, and S. P. Willner, 2005: Mid-Infrared Selection of Active Galaxies. *ApJ*, **631**, 163–168.

Stewart, K. R., T. Kaufmann, J. S. Bullock, E. J. Barton, A. H. Maller, J. Diemand, and J. Wadsley, 2011: Orbiting Circumgalactic Gas as a Signature of Cosmological Accretion. *ApJ*, **738**, 39.

Trainor, R. and C. C. Steidel, 2013: Constraints on Hyperluminous QSO Lifetimes via Fluorescent Lyα Emitters at Z ˜= 2.7. *ApJL*, **775**, L3.

Trainor, R. F. and C. C. Steidel, 2012: The Halo Masses and Galaxy Environments of Hyperluminous QSOs at z ˜= 2.7 in the Keck Baryonic Structure Survey. *ApJ*, **752**, 39.

Tumlinson, J., C. Thom, J. K. Werk, J. X. Prochaska, T. M. Tripp, D. H. Weinberg, M. S. Peeples, J. M. O'Meara, B. D. Oppenheimer, J. D. Meiring, N. S. Katz, R. Davé, A. B. Ford, and K. R. Sembach, 2011: The Large, Oxygen-Rich Halos of Star-Forming Galaxies Are a Major Reservoir of Galactic Metals. *Science*, **334**, 948–.

Turner, M. L., J. Schaye, C. C. Steidel, G. C. Rudie, and A. L. Strom, 2015: Detection of hot, metal-enriched outflowing gas around $z \approx 2.3$ star-forming galaxies in the Keck Baryonic Structure Survey. *MNRAS*, **450**, 2067–2082.

Veilleux, S., M. Meléndez, E. Sturm, J. Gracia-Carpio, J. Fischer, E. González-Alfonso, A. Contursi, D. Lutz, A. Poglitsch, R. Davies, R. Genzel, L. Tacconi, J. A. de Jong, A. Sternberg, H. Netzer, S. Hailey-Dunsheath, A. Verma, D. S. N. Rupke, R. Maiolino, S. H. Teng, and E. Polisensky, 2013: Fast Molecular Outflows in Luminous Galaxy Mergers: Evidence for Quasar Feedback from Herschel. *ApJ*, **776**, 27.

Venemans, B. P., H. J. A. Röttgering, G. K. Miley, W. J. M. van Breugel, C. de Breuck, J. D. Kurk, L. Pentericci, S. A. Stanford, R. A. Overzier, S. Croft, and H. Ford, 2007: Protoclusters associated with z > 2 radio galaxies . I. Characteristics of high redshift protoclusters. *A & A*, **461**, 823–845.

Voit, G. M., M. Donahue, G. L. Bryan, and M. McDonald, 2015: Regulation of star formation in giant galaxies by precipitation, feedback and conduction. *Nature*, **519**, 203–206.

Weiner, B. J., A. L. Coil, J. X. Prochaska, J. A. Newman, M. C. Cooper, K. Bundy, C. J. Conselice, A. A. Dutton, S. M. Faber, D. C. Koo, J. M. Lotz, G. H. Rieke, and K. H. R. Rubin, 2009: Ubiquitous Outflows in DEEP2 Spectra of Star-Forming Galaxies at z = 1.4. *ApJ*, **692**, 187–211.

Werk, J. K., J. X. Prochaska, J. Tumlinson, M. S. Peeples, T. M. Tripp, A. J. Fox, N. Lehner, C. Thom, J. M. O'Meara, A. B. Ford, R. Bordoloi, N. Katz, N. Tejos, B. D. Oppenheimer, R. Davé, and D. H. Weinberg, 2014: The COS-Halos Survey: Physical Conditions and Baryonic Mass in the Low-redshift Circumgalactic Medium. *ApJ*, **792**, 8.

Worseck, G., J. X. Prochaska, J. F. Hennawi, and M. McQuinn, 2016: Early and Extended Helium Reionization over More Than 600 Million Years of Cosmic Time. *ApJ*, **825**, 144.

Zakamska, N. L., M. A. Strauss, J. H. Krolik, M. J. Collinge, P. B. Hall, L. Hao, T. M. Heckman, Ž. Ivezić, G. T. Richards, D. J. Schlegel, D. P. Schneider, I. Strateva, D. E. Vanden Berk, S. F. Anderson, and J. Brinkmann, 2003: Candidate Type II Quasars from the Sloan Digital Sky Survey. I. Selection and Optical Properties of a Sample at 0.3 LT Z LT 0.83. *AJ*, **126**, 2125–2144.